Structural Transition of Oil-Swollen Cylindrical Micelles of $C_{12}E_5$ in Water Studied by SANS

U. Menge, P. Lang,* and G. H. Findenegg

Stranski Laboratorium für Physikalische und Theoretische Chemie, Technische Universität Berlin, Strasse des 17. Juni 112, D-10623 Berlin, Germany

P. Strunz

Hahn-Meitner-Institut, Glienicker Strasse 100, 14109 Berlin, Germany

Received: August 1, 2002; In Final Form: December 3, 2002

The effect of added oil on the local structure of oil-swollen cylindrical micelles in the system $C_{12}E_5$ + decane + water was investigated by small-angle neutron scattering (SANS). The geometry of the aggregates was studied for fixed overall concentration of surfactant plus oil, $c_m = 7$ mg/mL, and increasing oil content α (the mass fraction of oil in the dispersed mixture of surfactant plus oil), to clarify the dependency of the apparent molar mass on α which was observed in a preceding light scattering study (*J. Phys. Chem. B* **1999**, *103*, 5768). There it was found that with increasing α at given c_m the molar mass of the micelles increases up to a maximum near $\alpha = 0.07$ and then decreases sharply as the oil content is further increased. The present work shows that this decrease of the molar mass results from a decrease of the micellar contour length L_c, whereas the mass per unit length M_L of the aggregates increases almost linearly over the entire range of oil content.

Introduction

Amphiphilic molecules self-assemble into micelles of various geometries in water. The micellar shape is determined primarily by the effective cross-sectional area of the hydrophilic and hydrophobic moieties of the molecules. Surfactants with large water-soluble headgroups and small nonpolar tails tend to pack into aggregates of highest curvature, i.e., spherical micelles. Micellar shapes of lower mean curvature, such as elongated ellipsoids or oblate shapes will be favored, if the two moieties of the amphiphile have similar cross-sectional areas. For the particular case of $C_{12}E_5$ in water, it is well-established[1−5] that cylindrical micelles are present in the isotropic solution at ambient temperature. These cylindrical micelles can solubilize moderate amounts of oils,[6−9] as is visualized in Figure 1. The phase behavior and the structures of such ternary microemulsions have been the subject of an enormous number of publications.[10] In the present contribution, we focus on the structural transition from cylindrical micelles to globular oil-swollen droplets brought about by an increase of the oil content in the mixture as reported in two preceding contributions.[6,7]

Following the notation introduced in that work, we use the symbol c_m for the overall concentration of surfactant plus oil, $c_m = (m_s + m_o)/V$, where m_s and m_o is the mass of the surfactant and the oil respectively, and the mass fraction of oil in the solute mixture is denoted by the symbol $\alpha = m_o/(m_s + m_o)$. Using light scattering, we have investigated the effect of decane on the micellar shape of $C_{12}E_5$ in water. It was found that at overall concentrations c_m up to ca. 100 mg/mL an increase of the oil content up to $\alpha \approx 0.07$ causes a gradual increase of the molar mass of the aggregates. However, as α is further increased at constant c_m, the molar mass decreases sharply and a droplet microemulsion is eventually formed at $\alpha \geq 0.25$. The aim of the present work is to understand the structural transformations of the oil-swollen cylindrical micelles in the region $\alpha \leq 0.15$. Specifically, we wish to elucidate the reasons for the nonmonotonic change of the molar mass on increasing oil content.

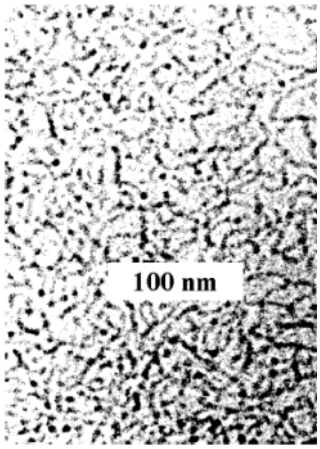

Figure 1. Cryo transmission electron micrograph of a vitrified $C_{12}E_5$ + decane + water mixture containing an overall concentration $c_m = 0.1$ g/mL of the solute with an oil fraction of $\alpha = 0.10$. The temperature prior to vitrification was 22 °C.

According to the flexible-surface model,[11] the surfactant monolayer separating the aqueous region from the oil domain can be regarded as a flexible membrane. The bending free energy per unit area f_B of this membrane, the minimum of which determines the shape of the micelle, is given by

$$f_B \propto \int (2\kappa(H - C_0)^2 + \bar{\kappa}K)\, dS \qquad (1)$$

* To whom correspondence should be addressed. Permanent address: Forschungszentrum Jülich, Institut für Festkörperforschung 52425 Jülich, Germany. E-mail: p.lang@fz-juelich.de.

10.1021/jp021797e CCC: $25.00
Published on Web 01/21/2003

where H and K represent the mean curvature and the Gaussian curvature, respectively, given by $H = (1/R_1 + 1/R_2)/2$ and $K = (R_1R_2)^{-1}$, with R_1 and R_2 the two principal radii of curvature. C_0 is the spontaneous curvature, and κ and $\bar{\kappa}$ are the curvature elasticity moduli of the membrane.[12] For a given system at a given temperature, f_B depends only on the radii R_1 and R_2 and thus on the geometry of the aggregate. In this case, the free energy will decrease if the radii increase, provided that the spontaneous curvature is sufficiently small. Accordingly, solubilization of oil in the cylindrical micelles should cause an increase of the micellar diameter rather than an increase of the contour length of the micelles.

To test this prediction, we studied the structural transition of the present system by small-angle neutron scattering (SANS). In the analysis of the scattering data, different routes were pursued. Following the work of Schurtenberger et al.,[13,14] a Guinier-type extrapolation of the SANS data for wormlike micelles was performed which yields a measure of the mass per unit length, M_L, and the cross-section radius of gyration $R_{g,cs}$ of the micelles, and allows to calculate their contour length L_c. A method for a quantitative analysis of the scattering data by nonlinear least-squares fitting of an appropriate scattering function was suggested by Pedersen and Schurtenberger.[15,16] On the basis of the work of Sharp and Bloomfield,[17] they derived a parametrized approximate expression for the scattering function of cylindrical micelles. In this treatment, the expression for the scattering function of a polymer chain with excluded volume, $S_{exv}(q,L_c,b)$, is combined with a term that takes into account the local stiffness of the chain, $S_{loc}(q,L_c,b)$, and the sum of these terms is multiplied with the scattering function of the cylinder cross-section, S_{cs} (q,R_{cs}). Here $q = 4\pi \sin(\theta/2)/\lambda$ is the scattering vector, with θ the scattering angle and λ the wavelength, b is the Kuhn segment length, and R_{cs} is the cylinder cross-section radius. Unfortunately, this promising formalism could not be implemented for the analysis of the present data, as will be explained in the discussion below. Instead, we constructed a new scattering function based on an expression by Koyama[18] which had been used successfully in the past to represent the scattering from semi-flexible polymer chains.[19−21] As is well-known, the Koyama expression does not take into account excluded-volume effects of the chain, and there has been some controversy about its accuracy in the intermediate q-range.[15,22,23] Accordingly, the results for the Kuhn segment length derived by this approach may be subject to a systematic error. However, despite this drawback, this approach offers a reasonably quantitative framework to analyze the way in which the oil-swollen cylindrical micelles transform into a droplet microemulsion as the oil content of the system is increased.

Experimental Section

Materials. The surfactant $C_{12}E_5$ was purchased from Nikko Chemicals Co., Japan, with a purity better than 99% according to the manufacturer. Decane (>98%) and D_2O (>99.9%) were purchased from Sigma-Aldrich Fine Chemicals, Germany. All substances were used without further purification.

Small-Angle Neutron Scattering. Small-angle neutron scattering experiments were performed at the instrument V4 of the Berlin Neutron Scattering Center BENSC at the HMI, Berlin, Germany. Neutrons were derived from a hydrogen cold source and monochromatized by a velocity selector. The mean de Broglie wavelength was set to $\lambda_0 = 0.6$ nm with a full width at half-maximum, fwhm, of the distribution $\Delta\lambda/\lambda_0 = 0.1$. The instrument was equipped with a 64 × 64 element ^{3}He detector with a pixel size of 10 × 10 mm^2, which was positioned at three different sample-to-detector distances (1, 4, and 16 m) to cover a range of scattering vectors 0.03 nm^{-1} ≤ q ≤ 3.6 nm^{-1} after radial averaging. Solutions for the scattering experiments were prepared by weight and contained in cylindrical quartz cells with a path length of 1 mm. We investigated a series of solutions with a fixed overall concentration of the solute c_m = 7 mg/mL in which the oil content was adjusted to $\alpha = 0$, 0.02, 0.05, 0.07, 0.10, and 0.15. Temperature control with an accuracy of ±0.2 K was achieved by an externally controlled water bath thermostat. Sampling times were chosen such that the statistical error was smaller than 2% at any scattering vector. Data reduction and calibration of intensities to absolute scale, using water as a standard scatterer, was achieved by HMI standard procedures according to Strunz et al.[24] The software packages ITP and DEC by Glatter[25,26] were applied to derive the scattering length density profile of the micellar cross-section.

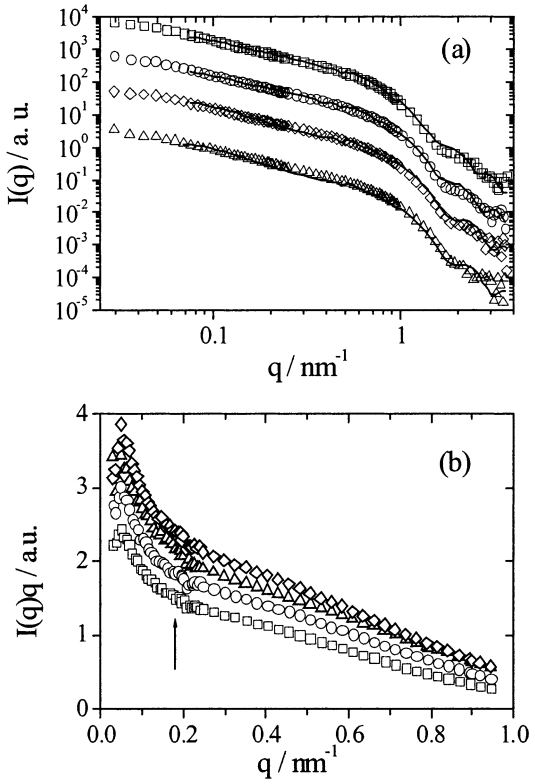

Figure 2. (a) Radially averaged SANS curves recorded at 22 °C, corrected for background and solvent scattering. The overall solute concentration was c_m = 7 mg/mL and the oil content α of the solute was (△) 0.02, (◇) 0.05, (○) 0.07, and (□) 0.10. The individual curves have been shifted on the ordinate by a factor of 10 with respect to the next below. The solid lines represent the best fit with the model function given in eq 7. (b) Cassasa-Holtzer plot of the same experimental data in the q-range relevant for the crossover from the rodlike to coil behavior at $q_c l_p \approx 1.9$ as indicated by the arrow.

Results and Discussion

The radially averaged, background and solvent corrected scattering curves for four samples of increasing oil content are displayed in Figure 2. In this double logarithmic representation, the scattering curves begin with a power-law range at low q-vectors, where $I(q) \propto q^{-x}$ with $x > 1$ and the global structure of the micelles dominates the scattering behavior. In the q-range in which the experiment is sensitive to the local cylindrical structure of the particles, the scattered intensity scales with an exponent $x = 1$. The crossover from power-law to the linear region is expected to occur at $q_c l_p \approx 1.9$,[20,27] where l_p is the

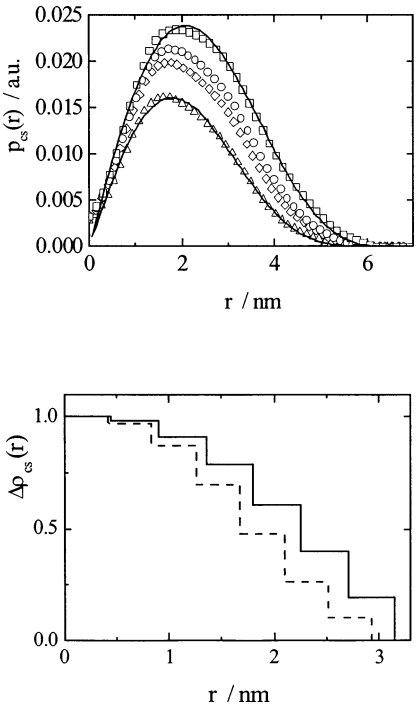

Figure 3. Top: Pair distance distribution functions calculated by indirect Fourier transformation from the scattering curves displayed in Figure 2. Symbols represent different oil contents of the solute α: (△) 0.02, (◇) 0.05, (○) 0.07, and (□) 0.10. The full lines are reconstructions of the PDD function according to the scattering length density profiles displayed on the bottom. Bottom: Excess scattering length density profiles for $\alpha = 0.02$ (dashed) and $\alpha = 0.10$ (full). The SLD profiles are normalized to unity at $r = 0$.

persistence length. Because the q^{-1}-regime cannot be identified unambiguously in the present case, this crossover cannot be determined from this representation. If the intensity is plotted in a Cassasa-Holtzer[28−30] or bending rod plot as $I(q)q$ vs q, the crossover is more evident[31] and the persitence length can be estimated to be roughly $l_p \approx 13$ nm with an uncertainty of about 2 nm for all samples investigated (see Figure 2b). At the high-q end of the linear regime, the scattering curves display an exponential decay as the experiment probes the cross-sectional structure of the micelles. In Figure 2a, the deviation from the linear q-dependence as well as the position of the first local minimum of the scattered intensity are shifted slightly to smaller scattering vectors as the oil-content of the solute increases, indicating qualitatively that the cross-sectional diameter of the micelles grows upon the addition of oil.

To quantify this observation we have analyzed the scattering data at scattering vectors $q \geq 0.2$ nm^{-1}, where the local cylindrical structure of the micelles dominates the scattering behavior, using the software packages ITP and DEC by Glatter.[25,26] For cylindrical particles, it is possible to calculate the pair-distance distribution (PDD) function $p_{cs}(r)$ of the cross-section by the indirect Fourier transform algorithm implemented in ITP. In a similar procedure, the radial excess scattering length density (SLD) profile $\Delta\rho_{cs}(r)$ of the cross-section is deduced from $p_{cs}(r)$. Figure 3 shows the PDD functions corresponding to the scattering curves displayed in Figure 2. The corresponding SLD profiles are displayed as well. From both functions, $p_{cs}(r)$ and $\Delta\rho_{cs}(r)$, it is obvious that the cross-sectional dimension of the micelles increases with increasing oil content α. The same trend has been observed in the system $C_{12}E_5$ + water + *n*-octane by cryo-transmission microscopy by Bernheim-Groswasser et al.[32] The analysis of our SANS-data allows us to quantify this

TABLE 1: Results of the Guinier Extrapolation of SANS Data for Solutions with a Solute Content of 7 mg/mL[a]

α	0.00	0.02	0.05	0.07	0.10	0.15
$\Delta\rho^2_m$ /10^{21} cm^2 g^{-2}	4.16	4.24	4.34	4.40	4.51	4.67
T	19 °C	19 °C	19 °C	19 °C	19 °C	19 °C
M_L/10^{-20} g nm^{-1}	1.13	1.23	1.41	1.53	1.75	2.04*
$R_{g,cs}$/nm	1.91	1.98	2.06	2.14	2.30	2.47*
M_W/10^6 g mol^{-1}	1.91			2.08	1.49	
L_c/nm	280			226	141	
†$R_{g,cs}$/nm	1.58	1.63	1.73	1.79	1.90	2.04*
T	22 °C	22 °C	22 °C	22 °C	22 °C	22 °C
M_L/10^{-20} g nm^{-1}	1.12	1.23	1.46	1.55	1.78	2.14*
$R_{g,cs}$/nm	1.87*	1.98	2.02	2.09	2.27	2.43*
M_W/10^6 g mol^{-1}	2.59	2.88	3.17	3.48	2.64	1.37
L_c/nm	384	388	360	372	246	106
†$R_{g,cs}$/nm	1.59*	1.65	1.74	1.77	1.88	2.02*

[a] The oil content of the solute is denoted α, M_L is the mass per unit length, and $R_{g,cs}$ is the cross-sectional radius of gyration. M_W is the mass-average molar mass measured by light scattering.[6,7] The contour length L_c of the aggregates was calculated according to $L_c = M_W/(M_L N_A)$. The values with the asterisk are extrapolated from the corresponding data at different α. The values calculated from eq 2 are marked by †.

observation by calculating the cross-section radius of gyration, $R_{g,cs}$, for the PDD via

$$R_{g,cs} = \left(\frac{\int_0^\infty r^2 p_{cs}(r)\, dr}{2\int_0^\infty p_{cs}(r)\, dr} \right)^{1/2} \tag{2}$$

The resulting values for $R_{g,cs}$ are summarized in Table 1.

We further analyzed the scattering curves according to the procedure suggested by Schurtenberger et al.[13,14] At sufficiently large values of q, the micelles scatter like cylinders of contour length L_c, the particle scattering factor of which can be factorized into a length contribution $P_{Lc}(q) \propto \pi/(qL_c)$ and a contribution of the cross-section $P_{cs}(q)$. As to be seen from Figure 3, the cross-sectional SLD profiles of the micelles are monotonic. In this case, we can apply the Guinier approximation to the cross-sectional particle scattering factor, i.e., $P_{cs}(q) \propto \exp\{-R_{g,cs}^2 q^2/2\}$, where $R_{g,cs}$ is the radius of gyration of the cross-section. Accordingly, the scattered intensity on absolute scale can be written as

$$I(q) \approx \Delta\rho_m^2 c_m \frac{M_L \pi}{q} \exp(-R_{g,cs} q^2/2) \tag{3}$$

Here $M_L = M_w/(N_A L_c)$ is the absolute mass per unit length of the micelles, M_w is the mass-average molar mass, L_c the contour length, and N_A is the Avogadro constant. The contrast factor per unit mass $\Delta\rho_m^2$ is given by

$$\Delta\rho_m^2 = \left(\frac{\sum b_c}{m_c} - \frac{\sum b_s}{m_s} \frac{\rho_s}{\rho_c} \right)^2 \tag{4}$$

where the subscripts c and s specify the cylindrical micelle and the solvent, respectively, $\sum b_i$ is the sum of the coherent scattering lengths of all molecules constituting the respective compound, m_i is the mass of molecule i, and ρ_i the respective mass density.

According to eq 3, a plot of $\ln(I(q)q)$ versus q^2 should be linear in the q-range where this approximation applies, and the cross-section radius of gyration $R_{g,cs}$ can be obtained from the slope of this linear dependence. Further, M_L can be calculated from the intercept of the linear extrapolation to $q = 0$. As a representative example, Figure 4 shows the cross-section Guinier

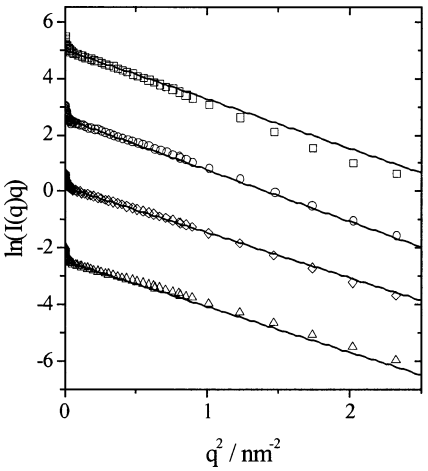

Figure 4. Cross-sectional Guinier plot of the SANS data displayed in Figure 2. The solute concentration was $c_m = 7$ mg/mL, and the oil content α was (△) 0.02, (◇) 0.05, (○) 0.07, and (□) 0.10. The individual curves are shifted on the ordinate by a factor of ln 10 with respect to the next below. The solid straight lines were obtained by linear least-squares fitting of the data in the range $0.05\ \text{nm}^{-2} \le q^2 \le 0.2\ \text{nm}^{-2}$.

plot of the scattering curves displayed in Figure 2. The values of $R_{g,cs}$ and M_L obtained by linear least-squares fitting of the data in the range $0.05\ \text{nm}^{-2} \le q^2 \le 0.2\ \text{nm}^{-2}$ are listed in Table 1.

In the Guinier analysis presented above, the contour length of the cylinders L_c was derived indirectly from M_L, using complementary information from the previous light scattering study.[6,7] We have attempted to derive L_c directly from the SANS data using the formalism of Pedersen and Schurtenberger.[15] However, we were unable to implement this formalism, as the expression for $S_{exv}(q,L_c,b)$ given in eq 13 of ref 15 yields physically meaningless (negative) values for $qR_g < 1$, where R_g is the overall radius of gyration of the cylinder. This inconsistency is not removed entirely when the crossover function $\omega(qR_g)$, which is used to link the Debye function for a flexible coil with an expansion that accounts for the excluded volume in eq 13 of ref 15, is replaced with $(1 - \omega(qR_g))$. In view of this unphysical behavior of $S_{exv}(q,L_c,b)$ in the low-qR_g limit, and also in view of the fact that this formalism involves a total of 13 model parameters which have to be determined beforehand by comparison with simulated scattering functions, we did not use the formalism of Pedersen and Schurtenberger in the present analysis. Instead, we constructed a modified particle scattering factor $P(q,L_c,b,U,R_{cs})$ along the ideas of these authors. In this new formalism, the finite cross-section diameter of the cylinders is taken into account by multiplying $P_{wlc}(q,L_c,b,U)$, the particle scattering factor of polydisperse wormlike chains,[18,20] with $P_{cs}(q,R_{cs})$, the cross-section form factor of a rigid homogeneous cylinder, i.e.

$$P(q,L_c,b,U,R_{cs}) = P_{wlc}(q,L_c,b,U)P(q,R_{cs}) \qquad (5)$$

where U is the polydispersity index of the contour length and

$$P_{cs}(q,R_{cs}) = \left[\frac{2J_1(qR_{cs})}{qR_{cs}}\right]^2 \qquad (6)$$

where R_{cs} is the cross-section radius and $J_1(qR_{cs})$ is the first-order Bessel function. To compare eq 5 to experimental data, it was multiplied with an amplitude $I(q = 0)$ and smeared with a Gaussian-type resolution function $R(q,\bar{q})$ as suggested by Pedersen[33] to give

$$I_{model}(q) = \int_0^\infty I(q = 0)P(q,L_c,b,U,R_{cs})R(q,\bar{q})\,dq \qquad (7)$$

where $\bar{q}$ is the nominal mean scattering vector. As Koyama's particle scattering factor of a wormlike chain contains an integration, which can be solved only numerically,[18] and because we take into account length polydispersity and experimental smearing, the solution of eq 7 requires three numerical integrations which makes the least-squares fitting rather time-consuming. To fasten the procedure, we fixed the polydispersity index to $U = 2$. Representative examples for the fits are shown as full lines in Figure 2a, and the resulting values of the parameters are summarized in Table 2.

TABLE 2: Results of the Linear Least Squares Fitting of eq 7 to SANS Data for Solutions with a Solute Content of 7 mg/mL[a]

α	0.00	0.02	0.05	0.07	0.10	0.15
T	19 °C	19 °C	19 °C	19 °C	19 °C	19 °C
L_c/nm	283	280	273	232	187	
b/nm	27.2	26.0	29.7	27.0	34.0	
$R_{g,cs}$/nm	1.39	1.45	1.45	1.70	1.89	2.08*
T	22 °C	22 °C	22 °C	22 °C	22 °C	22 °C
L_c/nm		350	332	386	253	
b/nm		22.0	25.0	27.0	30.2	
$R_{g,cs}$/nm	1.34*	1.45	1.58	1.69	1.83	2.06*

[a] The oil content of the solute is denoted α, L_c is the contour length, and b is the segment length. The cross-sectional radius of gyration $R_{g,cs}$ was calculated from the fitting parameter $R_{cs}^2 = 5/2R_{g,cs}^2$. The values with the asterisk are extrapolated from the corresponding data at different α.

As to be seen from Tables 1 and 2, the values for the contour length derived with different methods agree reasonably well. The segment lengths obtained by the fitting procedure are also in good agreement with the estimate for the persistence length, as $b = 2l_p$. The values for the cross-section radius of gyration, $R_{g,cs}$ resulting from the three methods differ somewhat (up to ca. 50%). However, if $R_{g,cs}$ is plotted as a function of the oil content α all methods yield a linear dependence with similar slopes. Therefore, the results obtained by the different methods may be regarded mutually consistent.

The main result of the present work is that $R_{g,cs}$ and the mass per unit length M_L of the micelles exhibit a monotonic increase with the oil content α over the entire experimental range. Up to $\alpha \approx 0.07$, the overall molar mass of the micelles M_w reflects this increase of M_L with the oil content, which implies that the contour length L_c of the micelles remains nearly constant in this region. The pronounced decrease of M_w observed at higher oil contents ($\alpha > 0.07$) thus implies a sharp decrease of the contour length as the oil content is further increased. These opposite trends of M_L and L_c and the resulting nonmonotonic dependence of M_w on α are shown in Figure 5. The pronounced decrease of L_c with increasing α at high oil contents eventually leads to the crossover from oil-swollen cylindrical micelles to spherical microemulsion droplets at $\alpha \ge 0.25$.[6]

A second remarkable trend indicated by the present results concerns the temperature dependence of the parameters M_L, M_w, and L_c. For given values of c_m and α, the molar mass M_w exhibits a pronounced temperature dependence.[7] On the other hand, $R_{g,cs}$ and the mass per unit length are virtually independent of temperature in our experiments. This appears to be a general behavior, as in the system $C_{12}E_5$ + water + *n*-octane the cross-sectional dimension is also found to be almost temperature invariant.[32] Accordingly, the finding that M_L is nearly independent of temperature (Table 1) also implies that the aggregates

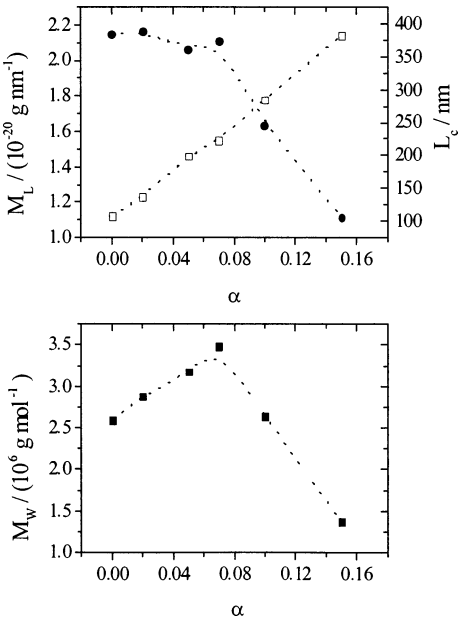

Figure 5. Mass per unit length M_L (□) and contour length L_c (●) (top) and mass-average molar mass M_w (bottom) as a function of the oil content α at $T = 22$ °C. The dotted lines are guides to the eye.

grow drastically in length when the temperature increases, as is nicely confirmed by the overall contour length values obtained from the model fits.

Conclusions

We have used SANS to determine the cross-section radius of gyration $R_{g,cs}$ and the mass per unit length M_L of oil-swollen cylindrical micelles in the water-rich corner of the $C_{12}E_5$ + decane + water phase diagram. We used simple asymptotic extrapolation and Glatter's indirect Fourier transform method, as well as elaborate nonlinear least-squares fitting to analyze the data. All of the three methods gave consistent results. By combining these data with results from light scattering,[6,7] we calculated the contour length L_c of the aggregates. It is found that M_L increases in a monotonic manner with the relative oil content α of the surfactant + oil solute mixture, as to be expected on the basis of the flexible-surface model.[11] Up to $\alpha = 0.07$, the contour length L_c of the cylindrical aggregates remains nearly constant, but a sharp decrease of L_c occurs as α exceeds 0.10. This decrease of L_c outweighs the further increase of the cross-sectional dimension, thus leading to a pronounced maximum of the micellar mass at about $\alpha \approx 0.07$. The sharp decrease of the contour length at $\alpha > 0.07$ supports the explanation by Menes et al.[34] for the existence of a closed-loop two phase-liquid/liquid region within the isotropic micellar phase of the microemulsion phase diagram.[35] According to Menes et al., the re-entrant phase behavior at constant temperature is due to a delicate balance of the weak attractive potential between large aggregates, leading to phase separation, and an increasing entropy term which leads to homogenization upon the addition of sufficiently large amounts of oil. The entropy gain is assumed to be due to the formation of smaller aggregates, as it was indeed observed in the present contribution.

Acknowledgment. We thank H. Mays for preparing cryo-TEM micrographs of the oil-swollen micelles (Figure 1) and Profs. J. Dhont and G. Nägele for helpful discussion. This work was supported by the Deutsche Forschungsgemeinschaft through Sfb 448.

References and Notes

(1) Brown, W.; Pu, Z.; Rymden, R. *J. Phys. Chem.* **1988**, *92*, 6086.
(2) Kato, T.; Anzai, S.; Takano, A.; Seimiya, T. *J. Chem. Soc., Faraday Trans. 1* **1989**, *85*, 2499.
(3) Kato, T.; Anzai, S.; Seimiya, T. *J. Phys. Chem.* **1990**, *94*, 7255.
(4) Li, X.; Lin, Z.; Cai, J.; Scriven, L. A.; Davis, H. T. *J. Phys. Chem.* **1995**, *99*, 10865.
(5) Glatter, O.; Strey, R.; Schubert, K.-V.; Kaler, E. W. *Ber. Bunsen-Ges. Phys. Chem.* **1996**, *100*, 323.
(6) Menge, U.; Lang, P.; Findenegg, G. H. *J. Phys. Chem. B* **1999**, *103*, 5768.
(7) Menge, U.; Lang, P.; Findenegg, G. H. *Coll. Surf. Sci. A* **2000**, *163*, 81.
(8) Brunner-Popela, J.; Mittelbach, R.; Strey, R.; Kaler, E. W.; Glatter, O. *J. Chem. Phys.* **1999**, *110*, 10623.
(9) Hellweg, T.; von Klitzing, R. *Physica A* **2000**, *283*, 349.
(10) For an overview, see: Hellweg, T. *Current Opinion in Colloid and Interface Science* **2002**, *7*, 50 and references given therein.
(11) Gompper, G.; Schick, M. Self-Assembling Amphiphilic Systems. In *Phase Transitions and Critical Phenomena*; Domb, C., Lebovitz, C., Eds.; Academic Press: London, 1994; Vol. 16.
(12) Helfrich, W. *Z. Naturforsch.* **1973**, *28c*, 693.
(13) Schurtenberger, P.; Magid, L. J.; King, S. M.; Lindner, P. *J. Phys. Chem.* **1991**, *95*, 4173.
(14) Schurtenberger, P.; Jerke, G.; Cavaco, C.; Pederson, J. S. *Langmuir* **1996**, *12*, 2433.
(15) Pedersen, J. S.; Schurtenberger, P. *Maromolecules* **1996**, *29*, 7602.
(16) Pedersen, J. S.; Laso, M.; Schurtenberger, P. *Phys. Rev. E* **1996**, *54*, 5917.
(17) Sharp, P.; Bloomfield, V. A. *Biopolymers* **1968**, *6*, 1201.
(18) Koyama, R. *J. Phys. Soc. Jpn.* **1973**, *34*, 1029.
(19) Burchard, W. *Macromol. Chem.; Macromol. Symp.* **1988**, *18*, 1 and references given therein.
(20) Denkinger, P.; Burchard, W. *J. Polym. Sci. B Polym. Phys.* **1991**, *29*, 589.
(21) Shukla, P.; Cotts, P. M.; Miller, R. D.; Russell, T. P.; Smith, B. A.; Wallraff, G. M.; Baier, M.; Thiyagarajan, P. *Macromolecules* **1991**, *24*, 5606.
(22) Huber, K.; Burchard, W.; Bantle, S. *Polymer* **1987**, *28*, 863.
(23) Pötschke, D.; Hickl, P.; Ballauff, M.; Åstrand, P.; Pedersen, J. S. *Macromol. Theory Simul.* **2000**, *9*, 345.
(24) Strunz, P.; Saroun, J.; Keiderling, U.; Wiedenmann, A.; Przenioslo, R. *J. Appl. Crystallogr.* **2000**, *33*, 829.
(25) Glatter, O. *J. Appl. Crystallogr.* **1977**, *10*, 415.
(26) Glatter, O.; Hainisch, B. *J. Appl. Crystallogr.* **1984**, *17*, 435.
(27) Kirste, R. G.; Oberthür, R. C. In *Small-Angle X-ray Scattering*; Glatter, O., Kratky, O., Eds.; Academic Press: London, 1982.
(28) Casassa, E. F. *J. Chem. Phys.* **1955**, *23*, 596.
(29) Holtzer, A. *J. Polym. Sci.* **1955**, *17*, 432.
(30) Schmidt, M.; Paradossi, G.; Burchard, W. *Makromol. Chem.; Rapid Commun.* **1985**, *6*, 767.
(31) Jerke, G.; Pedersen, J. S.; Egelhaaf, S. U.; Schurtenberger, P. *Langmuir* **1998**, *14*, 6013.
(32) Bernheim-Groswasser, A.; Tlusty, T.; Safran, S. A.; Talmon, Y. *Langmuir* **1999**, *15*, 5448.
(33) Pedersen, J. S. *J. Appl. Cryst.* **1990**, *23*, 321.
(34) Menes, R.; Safran, S. A.; Strey, R. *Phys. Rev. Lett.* **1995**, *74*, 3399.
(35) Kahlweit, M.; Strey, R.; Busse, G. *J. Phys. Chem.* **1990**, *94*, 3881.